Soft Matter

Mechanical feedback links cell division and dynamics in growing cell collectives

Journal:	*Soft Matter*
Manuscript ID	SM-ART-10-2024-001230.R1
Article Type:	Paper
Date Submitted by the Author:	10-Dec-2024
Complete List of Authors:	Sinha, Sumit; Harvard University, SEAS Li, Xin; University of Texas at Austin Department of Chemistry, Chemistry Malmi-Kakkada, Abdul; Augusta University, Physics and Biophysics Thirumalai, Dave; The University of Texas System, Chemistry

Mechanical feedback links cell division and dynamics in growing cell collectives

Sumit Sinha[1], Xin Li[2], Abdul N Malmi-Kakkada[3], and D. Thirumalai[1,2]

[1]*Department of Physics, University of Texas at Austin, Austin, TX 78712, USA.*

[2]*Department of Chemistry, University of Texas at Austin, Austin, TX 78712, USA. and*

[3]*Department of Physics and Biophysics,*

Augusta University, Augusta, GA 30912, USA.

(Dated: January 9, 2025)

Abstract

Local stresses in a tissue, a collective property, regulate cell division and apoptosis. In turn, cell growth and division induce active stresses in the tissue. As a consequence, there is a feedback between cell growth and local stresses. However, how the cell dynamics depend on local stress-dependent cell division and the feedback strength is not understood. Here, we probe the consequences of stress-mediated growth and cell division on cell dynamics using agent-based simulations of a two-dimensional growing tissue. We discover a rich dynamical behavior of individual cells, ranging from jamming (mean square displacement, $\Delta(t) \sim t^{\alpha}$ with α less than unity), to hyperdiffusion ($\alpha > 2$) depending on cell division rate and the strength of the mechanical feedback. Strikingly, $\Delta(t)$ is determined by the tissue growth law, which quantifies cell proliferation, measuring the number of cells $N(t)$ as a function of time. The growth law ($N(t) \sim t^{\lambda}$ at long times) is regulated by the critical pressure that controls the strength of the mechanical feedback and the ratio between cell division-apoptosis rates. We show that $\lambda \sim \alpha$, which implies that higher growth rate leads to a greater degree of cell migration. The variations in cell motility are linked to the emergence of highly persistent forces extending over several cell cycle times. Our predictions are testable using cell-tracking imaging techniques.

I. INTRODUCTION

Cell growth, proliferation, and apoptosis are ubiquitous in biology, and play a crucial role in embryogenesis, tumorigenesis, and wound healing [1, 2]. The breakdown of strict control between cell division and apoptosis rates could lead to fatal diseases like cancer [3]. In cancer metastasis, the cells develop migratory phenotype and invade the surrounding tissues and organs [4]. Therefore, to understand the role of cell division and apoptosis numerous experiments have been performed both in two and three dimensions, which provide the time traces of cells [5–8]. The cell trajectories could be used to calculate dynamical properties of cells [9] that may be quantitatively compared with experiments [6]. By building on the understanding that cell division, apoptosis, and mechanical forces are fundamentally intertwined in tissue growth [5–8], we examine the complex feedback loop between these factors and its impact on cell dynamics. We employ agent-based simulations to model a two-dimensional growing tissue, which allows us to examine the consequences of varying cell division rate and the strength of mechanical feedback on the tissue and cell dynamics.

Our study centers on the concept of mechanical feedback, where the local stresses within a tissue directly influence the ability of cells to grow and divide. We elucidate the nuanced interplay between the rate of cell division and the strength of mechanical feedback in shaping the dynamics of the growing tissue which may have important consequences on understanding the emergent morphogical transitions. For instance, a growing tissue exhibits a morphological transition, characterized by contrasting collective cell dynamics in the pre-and post-transition phases [5]. Cells in the pre-transition phase exhibit fluid-like behavior whereas those in the post-transition phase are more solid-like [5]. The morphological transition, resulting in the contrasting dynamics, was attributed to the microenvironment-

dependent growth and proliferation of cells [5, 10]. The growth of cells in tissue depends on the local stresses, which in turn depend on the local growth rate. In other words, there is a feedback between local stress and cell growth, as was pointed out in a prescient study nearly two decades ago [10]. In addition to fluid and solid-like behavior, the dynamics could also show glassy behavior in confluent [11] and non-confluent tissues [12]. How the mechanical feedback and cell division affects the observed dramatic variations in collective cell dynamics as the tissue grows is largely unknown.

Previous studies that considered cell growth and division on the cell collective dynamics assumed that the birth rate of cells depends on its coordination number [13]. However, recent experiments report that mere contact between cells may not be sufficient for inhibiting mitosis in cells [5]. Here, building upon prior work [12, 14–17] where the growth of a cell depends on the local pressure, we establish that the dynamics of cells is linked to the tissue growth law. We show that tissue growth is controlled by two parameters- the critical pressure (p_c) and the cell birth rate (k_b, the inverse of the cell division time), which are intrinsic properties of individual cells. The p_c value determines the mechanical feedback strength [18].

The central results of this work are: (a) Depending on the values of p_c and k_b, cells can exhibit widely varying dynamics from subdiffusive (the mean-squared displacement, $\Delta(t) \propto t^{\alpha}, \alpha \leq 1$), to superdiffusive ($1 < \alpha \leq 2$) or even hyperdiffusive ($\alpha > 2$) dynamics. On increasing the value of p_c, the cells transition from sub-diffusive to hyperdiffusive dynamics. Surprisingly, on decreasing k_b, the cells switch from sub to super-diffusive or super to hyper-diffusive dynamics. (b) The tissue growth law, $N(t) \propto t^{\lambda}$, where N is the number of cells exhibits a power law increase in time (t). Strikingly, the global growth law is a predictor of the single-cell dynamics. As λ increases, so does α with $\alpha \sim \lambda$. (c) The emergence of

persistent forces due to cell division that extends over several cell cycle times is the principal reason for the anomalous (super or hyper-diffusive) cell dynamics. Our work provides a unifying framework for understanding origins of differing dynamical regimes (sub-diffusive [11], diffusive [13] and super-diffusive [12]) in the collective movement of cells driven by mechanical feedback arising from apoptosis and division.

II. METHODS

We briefly explain the off-lattice agent-based computational model used to simulate the spatio-temporal dynamics of a two-dimensional (2D) growing tissue. The computational model is adapted from previous studies [9, 12, 14–17, 19, 20]. The cells are represented as interacting deformable disks with radius depending on local rules, which assume that cells grow stochastically, and divide upon reaching a critical mitotic size (R_m). The interaction between cells is the sum of elastic and adhesive forces. We also assume that the cells are moving in an overdamped environment in which the inertia is negligible and viscous forces are large compared to environmental fluctuations.

Forces: The elastic (repulsive) force between two disks of radii R_i and R_j is modeled as,

$$F_{ij}^{el}(t) = \frac{h_{ij}^{3/2}(t)}{\frac{3}{4}\left(\frac{1-\nu_i^2}{E_i} + \frac{1-\nu_j^2}{E_j}\right)\sqrt{\frac{1}{R_i(t)} + \frac{1}{R_j(t)}}}, \tag{1}$$

where E_i and ν_i, respectively, are the elastic modulus and Poisson ratio of cell i. The overlap between the disks, if they interpenetrate without deformation, is h_{ij}, is defined as $\max[0, R_i + R_j - |\vec{r}_i - \vec{r}_j|]$ with $|\vec{r}_i - \vec{r}_j|$ being the center-to-center distance between the two disks.

Cell adhesion, mediated by receptors on the cell surface, enables the cells to stick together. For simplicity, we assume that the receptor and ligand molecules are evenly distributed on

the cell surface. Consequently, the magnitude of the attractive adhesive force, F_{ij}^{ad}, between two cells i and j scale as a function of their contact line segment, L_{ij}. Keeping the 3D model as a guide [12], we calculate F_{ij}^{ad} using,

$$F_{ij}^{ad} = L_{ij} f^{ad} \frac{1}{2}(c_i^{rec} c_j^{lig} + c_j^{rec} c_i^{lig}), \tag{2}$$

where the c_i^{rec} (c_i^{lig}) is the receptor (ligand) concentration (assumed to be normalized to the maximum receptor or ligand concentration so that $0 \leq c_i^{rec}, c_i^{lig} \leq 1$). In the present study, c_i^{rec}, c_j^{lig} are fixed and have been included for consistency with previous studies [12, 16, 17]. The coupling constant f^{ad} allows us to rescale the adhesion force to account for the variabilities in the maximum densities of the receptor and ligand concentrations. We calculate the contact length, L_{ij}, using the length of contact between two intersecting circles, $L_{ij} = \frac{\sqrt{(|4r_{ij}^2 R_i^2 - (r_{ij}^2 - R_j^2 + R_i^2)^2|)}}{r_{ij}}$. Here, r_{ij} is the distance between cells i and j. As before, R_i and R_j denote the radius of cell i and j. In the present case, the strength of repulsive interactions is very large compared to attractive forces which can be seen in Figure 1a.

The the sum of the repulsive and adhesive forces in Eqs.(1) and (2) point along the unit vector $\mathbf{n}_{ij}$ from the center of cell j to the center of cell i. The total force on the i^{th} cell is given by the sum over its nearest neighbors ($NN(i)$),

$$\mathbf{F}_i = \Sigma_{j \epsilon NN(i)} (F_{ij}^{el} - F_{ij}^{ad}) \mathbf{n}_{ij}. \tag{3}$$

The nearest neighbors satisfy the condition $R_i + R_j - |\mathbf{r}_i - \mathbf{r}_j| > 0$.

Equation of Motion: We used overdamped dynamics of the motion of the i^{th} cell. The equation of motion is,

$$\dot{\mathbf{r}}_i = \frac{\mathbf{F}_i}{\gamma_i}. \tag{4}$$

Here, γ_i is the friction coefficient of the i^{th} cell. We assume γ_i to be equal to $cR_i(t)$, where c is a constant. Note, we neglect temperature effects because the drag forces are high [13]

compared to environmental fluctuations.

Cell growth, division, and apoptosis: In the model, cells are either dormant (D) or in the growth (G) phase depending on the magnitude of the local pressure of the cell (see Figure 1b for a schematic). Using Irving-Kirkwood's definition, we calculate the pressure (p_i) on the i^{th} cell due to contact with its neighbors [21] using,

$$p_i = \frac{1}{2}\Sigma_{j\epsilon NN(i)}\frac{\mathbf{F}_{ij}\cdot\mathbf{dr}_{ij}}{A_i}, \tag{5}$$

where A_i is local area of influence, equal to $\theta\pi R_i^2$. The proportionality constant θ serves as a measure to sample the local area around the i^{th} cell and was chosen to be 1.5. If the local pressure on the i^{th} cell, p_i, exceeds a critical value (p_c) the cell immediately ceases to grow and enters the dormant phase. Note that the cell can switch to the growth phase once $\frac{p_i(t)}{p_c} < 1$. The critical pressure, p_c, serves as a mechanical feedback [10]. The local pressure, p_i, can easily exceed p_c if it is small. In this case, most cells would be dormant for a long time. In the opposite limit, $p_c \gg p_i$, it is unlikely that the cells would reach the dormant phase. This would result in cell proliferation. Thus, p_c determines the strength of the mechanical feedback. A previous study used p_c to control cell growth in confined spaces in a different context [18] and showed growth-driven jamming transition, controlled by the strength ($\propto \frac{1}{p_c}$) of the mechanical feedback. They did not consider cell dynamics, which is the focus of our investigation.

The threshold for cell dormancy (p_c) is a coarse-grained parameter that accounts for the processes inside a cell which detects intercellular interactions and provides feedback on the cell growth. One of the factors that inhibits cell proliferation is cell density, a phenomenon attributed to physical contact between cells. Contact inhibition of proliferation (CIP) describes the slowing down or cessation of cell proliferation at confluence [22]. This is evident from growth curves (i.e. increase in cell number versus time) that level off at

confluence, accompanied by biochemical indications of cell cycle arrest [23, 24]. This cell behavior motivated us to consider pressure as a mechanical feedback on cell growth and division.

For growing cells, we assume that the area increases at a constant rate r_A as the cell cycle progresses. The cell radius is updated from a Gaussian distribution with the mean rate $\dot{R} = (2\pi R)^{-1} r_A$. Over the cell cycle time τ, r_A is taken to be,

$$r_A = \frac{\pi (R_m)^2}{2\tau}, \tag{6}$$

where R_m is the mitotic radius. The cell cycle time is related to the growth rate (k_b) by $\tau = \frac{ln\ 2}{k_b}$. A cell divides once it grows to the fixed mitotic radius (R_m). To ensure the total area of a cell is conserved upon cell division, we use $R_d = R_m 2^{-1/2}$ as the radius of the daughter cells. The mother and daughter cells are placed at a center-to-center distance, $d = 2R_m(1 - 2^{-1/2})$ upon cell division. The direction of the new cell location is chosen randomly from a uniform distribution on the unit circle [12, 25]. One source of stochasticity in the cell movement is the random choice for the mitotic direction. The cells can also undergo apoptosis at rate k_a. In all the simulations, we vary k_b but the apoptosis rate (k_a) is fixed to $10^{-6} s^{-1}$. The values of the parameters used in the simulations are given in Table 1.

Table I: The parameters used in the simulations.

Parameters	**Values**	**References**
Timestep (Δt)	10s	This paper
Critical Radius for Division (R_m)	5 μm	[12, 15]
Friction coefficient ($\frac{\gamma_i}{R_i}$)	0.0942 kg/(μm s)	This paper
Cell Cycle Time (τ_{min})	54000 s	[12, 26–28]
Adhesive Coefficient (f^{ad})	$10^{-4}\mu$N/μm	This paper
Mean Cell Elastic Modulus (E_i)	10^{-3}MPa	[12, 29]
Mean Cell Poisson Ratio (ν_i)	0.5	[12, 15]
Death Rate (k_a)	10^{-6}s^{-1}	[12]
Mean Receptor Concentration (c^{rec})	1.0 (Normalized)	[12]
Mean Ligand Concentration (c^{lig})	1.0 (Normalized)	[12]

We initiated the simulations by placing 100 cells on a 2D plane whose coordinates are chosen from a normal distribution with zero mean, and standard deviation 25 μm. For each parameter set, 20 different simulations were performed and the observables reported here were averaged over these simulation runs. All the parameters except p_c and k_b are fixed. All the simulations are terminated when the scaled time $t^* = (k_b - k_a)t \sim 3.74$. A representative snapshot of the growing tissue is shown in Figure 1c.

Limitations of the model: We have modeled individual cells by a disc of radius r. The coupling between the cells is modeled by short ranged Hertzian interactions, which depends on the dynamical radius of the cell. In reality, the shape of a cell is anisotropic, and should be taken into account. Here, we focus on long-time, order of cell-division time, collective dynamics where the short time dynamics of cell shape fluctuations may not be as relevant.

III. RESULTS

A. Weaker mechanical feedback on cell division enhances cell motility

Typically cell division is associated with tissue volume growth due to increasing number of cells. In a growing cell collective where cells are tightly packed in space, local stress could regulate the propensity for cells to divide and in turn influence the cell dynamics. To assess the effect of mechanical feedback on cell dynamics, we varied p_c, which controls the strength of the mechanical feedback on cell division. Low p_c correspond to stronger mechanical feedback as the critical pressure threshold required for cells to enter the dormant state can be easily reached. On the other hand, high p_c values imply weaker mechanical feedback as local stress values will have to be larger to reach the critical pressure. To probe the connection between mechanical feedback and cell dynamics, we calculated the mean squared displacement ($\Delta(t)$),

$$\Delta(t) = \frac{1}{N}\sum_{i=0}^{i=N}[\mathbf{r}_i(t) - \mathbf{r}_i(0)]^2, \tag{7}$$

where $\mathbf{r}_i(t)$ is the position of the i^{th} cell at time t, and N is the number of cells whose positions were tracked. Because cells undergo apoptosis, we only tracked cells that were present throughout the simulations in this calculation. Figure 2a shows the time dependence of $\Delta(t)$ for three values of p_c (from strong feedback to weak): $10^{-5}Nm^{-1}, 10^{-4}Nm^{-1}$ and $10^{-3}Nm^{-1}$ at fixed $\frac{k_b}{k_a} = 20$. We analyzed the dynamics at two different timescales - intermediate ($t < \frac{1}{k_b - k_a}$) and long time limit ($t > \frac{1}{k_b - k_a}$) as compared to the average time it takes for a cell to divide. The effect of mechanical feedback on cell dynamics is highly dependent on the timescale we probe. In the intermediate time limit, the dynamics is subdiffusive ($\Delta(t) \sim t^{\delta}, \delta < 1$) irrespective of the p_c values. However, the long time dynamics strongly depends on the p_c. We find that $\Delta(t) \sim (t^*)^{\alpha}$ is subdiffusive ($\alpha = 0.68$) for $p_c = 10^{-5}Nm^{-1}$,

superdiffusive ($\alpha = 1.36$) for $p_c = 10^{-4} Nm^{-1}$ and hyperdiffusive ($\alpha = 3$) for $p_c = 10^{-3} Nm^{-1}$ (see Figure 2a Inset). Here, the time is normalized such that $t^* = (k_b - k_a)t$. Overall, we observe that as the mechanical feedback strength increases (realized by decreasing p_c) the cells are jammed, resulting in slow dynamics. Meanwhile, weaker mechanical feedback (larger p_c) gives rise to superdifussive or even hyperdiffusive dynamics. We anticipate that this cell dynamics behavior is directly related to the increased cell proliferation and the consequent growth of the cell collective size at lower mechanical feedback.

Next, we estimated the physical size of the cell collective using,

$$\Delta r(t) = \frac{1}{N_b(t)} \sum_{i=1}^{N_b} |\mathbf{r}_i(t) - \mathbf{R}(t)| \tag{8}$$

where $N_b(t)$ is the total number of boundary cells at time t and $\mathbf{R}(t)$ is the center of the cell collective at time t. These quantities can be readily measured using imaging experiments [5, 6]. The size of the cell collective increases algebraically with time, $\Delta r(t) \sim (t^*)^{\xi}$, where the parameter ξ characterizes the size growth of the cell collective. Figure 2b shows $\Delta r(t)$ for p_c equal to $10^{-5} Nm^{-1}, 10^{-4} Nm^{-1}$ and $10^{-3} Nm^{-1}$ with $\frac{k_b}{k_a} = 20$. We find that the size growth is maximal for $p_c = 10^{-3} Nm^{-1}$, similar to the cell dynamics behavior quantified using $\Delta(t)$. For $p_c = 10^{-5} Nm^{-1}, \xi = 0.34$, for $p_c = 10^{-4} Nm^{-1}, \xi = 0.68$ and for $p_c = 10^{-3} Nm^{-1}, \xi = 1.23$. We surmise from the behavior of $\Delta(t)$ and $\Delta r(t)$ that the tissue dynamics is enhanced with weaker mechanical feedback i.e. increasing p_c, for a fixed value of $\frac{k_b}{k_a}$. This is because of the higher probability that the cells can divide as p_c increases, as evident from the size growth of the cell collective.

To ascertain whether mechanical feedback is the main factor in controlling cell division and in turn cell dynamics, we varied the cell division rate. Given that cell dynamics is enhanced with weaker mechanical feedback at a fixed value of the cell division rate, we next wanted to understand how cell dynamics would be affected by varying the cell division

rate (k_b) at a fixed value of the mechanical feedback strength. We varied k_b and kept the apoptosis rate constant ($k_a = 10^{-6}s^{-1}$). Figure 2c shows $\Delta(t)$ for $\frac{k_b}{k_a} = 20, 8$ and 2 at a fixed $p_c = 10^{-4}Nm^{-1}$. Surprisingly, slower dividing cells have higher motility in the long time ($[k_b - k_a]t > 1$) limit. For $\frac{k_b}{k_a} = 20$, the MSD exponent values ($\Delta(t) \sim (t^*)^\alpha$ at long times), are $\alpha = 1.36$, for $\frac{k_b}{k_a}$ equal to 8, $\alpha = 1.67$ and for $\frac{k_b}{k_a}$ equal to 2, $\alpha = 2.90$. We observed a similar behavior whereby the size of the cell collective is larger for lower values of $\frac{k_b}{k_a}$ (see Fig. 2d). For $\frac{k_b}{k_a}$ equal to 20, $\xi = 0.68$, for $\frac{k_b}{k_a}$ equal to 8, $\xi = 0.85$ and for $\frac{k_b}{k_a}$ equal to 2, $\xi = 1.23$. The time dependent changes in $\Delta r(t)$ and $\Delta(t)$ shows that the degree of migration, quantified using ξ and α, is enhanced with decreasing cell division rate at fixed strength of mechanical feedback. We anticipate that this is due to slower dividing cells experiencing less local stress as compared to faster dividing cells. This shows that the interplay between mechanical feedback and cell division is the key regulator of cell dynamics as opposed to cell division rate alone.

B. Average time-dependent pressure relative to critical pressure explains how cell collective growth is determined by mechanical feedback

We next sought out to determine what is the unifying explanation for the non-trivial cell dynamics in a growing cell colony as mechanical feedback and division rate are varied? The answer lies in how the growth law responds to the mechanical feedback. The growth law is an emergent property that depends not only on the individual cell properties but also at the global cell collective scale, through the mechanical feedback and intercellular interactions. Depending on whether the average pressure experienced by cells exceeds or remain below the critical pressure, we obtain slower or faster number growth, which can be determined experimentally by counting the number of cells as a function of time [5].

Changing p_c: We first calculated the number of cells (N) as a function of time at $p_c = 10^{-5}Nm^{-1}, 10^{-4}Nm^{-1}$ and $10^{-3}Nm^{-1}$ with $\frac{k_b}{k_a} = 20$ (Figure 3a). We find that $N(t)$ increases as, $N(t) \sim t^{\lambda}$. For $p_c = 10^{-5}Nm^{-1}, \lambda = 1$, for $p_c = 10^{-4}Nm^{-1}$, $\lambda = 1.31$ and for $p_c = 10^{-3}Nm^{-1}$, $\lambda = 2.78$. It is clear that growth rate increases as the mechanical feedback strength decreases (Figure 3a). To determine the origin of the enhanced growth as p_c increases, we calculated the average pressure, $\langle p(t) \rangle = \frac{1}{N}\sum_{i=1}^{N} p_i$ (Figure 3b). For $p_c = 10^{-5}$, the average value of $\langle p(t) \rangle$ is always higher than the critical pressure, which implies that the cells are predominantly in the dormant phase. For $p_c = 10^{-4}$, $\langle p(t) \rangle$ initially exceeds p_c then dips below p_c and once again exceeds it after a few cell cycle times. This causes the cells to start entering dormancy. However, for $p_c = 10^{-3}$, $\langle p(t) \rangle$ is always smaller than p_c, implying that the majority of the cells are in the growth phase, resulting in increased cell division, and proliferation. Therefore, the average value of pressure relative to the critical pressure is a key parameter that determines the growth of the cell collective.

Changing $\frac{k_b}{k_a}$: Next, we obtained $N(t)$ at the fixed value of $p_c = 10^{-4}$ for three values of $\frac{k_b}{k_a} = 20, 8$ and 2 as shown in Figure 3c. The growth exponents ($N(t) \sim t^{\lambda}$) are $\lambda = 1.31$, $\lambda = 1.69$ and $\lambda = 2.60$ for $\frac{k_b}{k_a} = 20$, $\frac{k_b}{k_a} = 8$, $\frac{k_b}{k_a} = 2$, respectively. Strikingly, tissue growth rate decreases as cell division rate increases, which may be understood in terms of the dynamic changes in the average pressure, $\langle p(t) \rangle$, plotted in Figure 3d, as a function of $\frac{k_b}{k_a}$. For $\frac{k_b}{k_a} = 2$, the $\langle p(t) \rangle$ is smaller than p_c for long times (exceeding the cell division time) unlike the case for $\frac{k_b}{k_a} = 20$ and 8, indicating that the generation of pressure in the tissue is suppressed with lower $\frac{k_b}{k_a}$. We surmise that slower division rate allow cells to quickly rearrange their positions locally to minimize intercellular forces and lower the pressure. Therefore, cell division events are more prevalent when cells divide slowly as compared to those that divide fast, thus resulting in greater tissue growth. Interestingly, the pressure curve for $\frac{k_b}{k_a} = 2$,

shows large fluctuations because during cell division large pressure is generated momentarily, owing to the two daughter cells being in spatial proximity, in comparison to the average small pressure. Our analyses show that for both conditions (changing p_c and $\frac{k_b}{k_a}$), the mechanical feedback determines the cell division which in turn influences cell dynamics.

C. Growth law dictates cell dynamics

Our results so far suggest that the cell dynamics is determined by the tissue growth law. The generality of this result follows from the following arguments. If the overall shape of the tissue is circular in 2D (see Figure 1c), we expect the exponents governing the mean squared displacement α ($\Delta(t) \sim t^{\alpha}$) and the number growth λ ($N(t) \sim t^{\lambda}$) to have similar values. From the algebraic growth of the tissue, it follows that $N(t) \sim t^{\lambda} \sim r^2$, which holds for a circular shape. From the relation $r^2 \sim \Delta(t) \sim t^{\alpha}$, expect that $\alpha \sim \lambda$. In addition, the exponents ξ ($\Delta r(t) \sim t^{\xi}$) and λ should be related as $\lambda \approx 2\xi$. By comparing the exponents α and λ in Figure 4a, we note that the relation $\alpha \sim \lambda$ is approximately satisfied. Similarly, $\lambda \approx 2\xi$ as shown in the inset of Figure 4a.

Based on the findings in Figures 4a we are able to predict a diagram of states as a function of mechanical feedback strength (p_c) and cell division rate ($\frac{k_b}{k_b}$). Recent works probing the effect of cell division and apoptosis have reported subdiffusive [11], diffusive [13], and superdiffusive motion [12]. However, the regime in which these values emerge is unclear. Time traces of cell positions can be recorded using particle tracking techniques to quantify the features of cell dynamics. In anticipation of such experiments, we characterized single-cell dynamics by calculating the mean squared displacement over a broad range of p_c and $\frac{k_b}{k_b}$. As the value of α can be used to determine the nature of dynamics in the time regime of interest, we extracted the α exponent in the long time limit. Figure 4b shows

the two-dimensional diagram of states. Notably, we observe all three regimes of motion, subdiffusive, superdiffusive, and hyperdiffusive, by varying $\frac{k_b}{k_a}$ and p_c.

Figure 4b reveals three interesting characteristics of cell dynamics: (a) upon increasing p_c, there is a transition from subdiffusive to superdiffusive, and finally hyperdiffusive behavior. At fixed $\frac{k_b}{k_a} = 20$, for $p_c = 5 \times 10^{-6} Nm^{-1}$ dynamics is subdiffusive while for $p_c = 10^{-4} Nm^{-1}$ cells exhibit superdiffusive motion. Upon further increasing p_c to $10^{-3} Nm^{-1}$, hyperdiffusive dynamics is observed. (b) Surprisingly, upon decreasing $\frac{k_b}{k_a}$, α increases. For smaller p_c values, on decreasing $\frac{k_b}{k_a}$, the dynamics change from subdiffusive to superdiffusive behavior. For higher p_c values, the dynamics changes from superdiffusive to hyperdiffusive. For fixed $p_c = 10^{-5} Nm^{-1}$, the subdiffusive dynamics at $\frac{k_b}{k_a} = 20$ changes to superdiffusion at $\frac{k_b}{k_a} = 2$. For a higher value of $p_c = 10^{-4} Nm^{-1}$, at $\frac{k_b}{k_a} = 20$ ($\frac{k_b}{k_a} = 2$), the dynamics is superdiffusive (hyperdiffusive). The diagram of states (Figure 4b) was created using a smoothing procedure where the values of the MSD exponents at unknown values of $\frac{k_b}{k_a}$ and p_c were interpolated using the known simulation MSD values. The interpolation is logarithmically (linearly) scaled in p_c ($\frac{k_b}{k_a}$) axis. The two-dimensional phase diagram predicts the emergence of different dynamical regimes, from subdiffusive to hyperdiffusive, which can be tested in imaging experiments [5, 6].

D. Emergence of highly correlated force

Next, we wanted to gain a mechanistic understanding of the emergent anomalous dynamics of individual cells. We calculated the force autocorrelation function, $\mathrm{FAF}(t^*) = \frac{\langle \mathbf{F}(t+t^*) \cdot \mathbf{F}(t) \rangle_t}{\langle \mathbf{F}(t) \cdot \mathbf{F}(t) \rangle_t}$ [19], which in an overdamped system encodes the directed nature of motion in individual cells. Here, $\mathbf{F}(t)$ is the force on the cell at time t and $\langle ... \rangle_t$ is the time average. Figure 5 shows the plot of FAF for varying $p_c = 10^{-3} Nm^{-1}, 10^{-4} Nm^{-1}$ and $10^{-5} Nm^{-1}$ at

fixed $\frac{k_b}{k_a} = 20$. It shows that the FAF decays via a two steps, characterized by short ($\frac{\gamma}{ER_m}$) and long ($\sim \frac{1}{k_b - k_a}$) times. To extract the two-time scales, we fit FAF using $Ae^{-\frac{t^*}{\tau_c}} + C$ in both the regimes.

At short times (see the inset of Figure 5), for $p_c = 10^{-3} Nm^{-1}$, $A = 0.5, \tau_c = \frac{1.2\gamma}{ER_m}$ and $C = 0.41$. For $p_c = 10^{-4} Nm^{-1}$, $A = 0.75, \tau_c = \frac{0.97\gamma}{ER_m}$ and $C = 0.16$. Lastly, for $p_c = 10^{-5} Nm^{-1}$, $A = 0.81, \tau_c = \frac{0.95\gamma}{ER_m}$ and $C = 0.11$. It is clear that at short times, the relaxation time is approximately close to the elastic time scale $\frac{\gamma}{ER_m}$, which is negligible compared to $\frac{1}{k_b - k_a}$.

In the long time limit, the FAF exhibits correlations. For $p_c = 10^{-3} Nm^{-1}$, $A = 0.41, \tau_c = \frac{2.2}{k_b - k_a}$ and $C = -0.06$. For $p_c = 10^{-4}$, $A = 0.12, \tau_c = \frac{2.3}{k_b - k_a}$ and $C = -0.02$. Lastly, at strong mechanical feedback ($p_c = 10^{-5} Nm^{-1}$), $A = 0.04, \tau_c = \frac{0.2}{k_b - k_a}$ and $C \approx 0$. A is negligible, implying the absence of correlations force, which explains the observed subdiffusive dynamics. The value of A for $p_c = 10^{-3} Nm^{-1}$ is four times larger than for $p_c = 10^{-4} Nm^{-1}$. In addition, the FAF decays over (2-3) cell division times when the feedback strength is weak. Larger magnitude of FAF in the long time regime leads to higher degree of migration for $p_c = 10^{-3} Nm^{-1}$.

IV. CONCLUSION

We used simulations of a minimal two-dimensional off-lattice model to provide a comprehensive analysis of the variations in the cell dynamics and tissue growth as the strength of the mechanical feedback and cell division rates are altered. Building upon our earlier work showing the remarkable spatial and temporal variations in the dynamics of the cells from the center to the periphery of 3D cell collectives [12, 17], we discover that the interplay between mechanical feedback strength and cell number growth is a key determinant of

cell dynamics. The emergent dynamics of the cell collective changes from subdiffusive to superdiffusive to hyperdiffusive, as the p_c and $\frac{k_b}{k_a}$ are varied. We quantify the emergence of a force that is highly correlated in time arising from cell division that is persistent over several cell division times which is directly correlated with super-diffusive and hyper-diffusive cell dynamics. Notably, we show that biologically relevant parameters (p_c, $\frac{k_b}{k_a}$) could be chosen to suppress highly directed cell dynamics even as the cell division rate is increased.

In growing cell collectives, highly persistent forces emerge with weaker mechanical feedback on cell division whose decay exhibits two relaxation time scales: one short (elastic time scale, $\frac{\gamma}{ER_m}$) and one long (division-apoptosis time scale, $\frac{1}{k_b - k_a}$). The presence of persistent forces determines the variations in the dynamics as cell division rates and the strength of the feedback are varied. Weaker mechanical feedback corresponding to higher p_c values lead to more persistent force correlations which in turn results in hyperdiffusive cell dynamics.

How cell divisions affect tissue fluidity and how long-lasting and reversible is this effect are outstanding questions of broad relevance to collective cell behaviors [30]. We discover that the cell dynamics is controlled by the growth law of the cell collective, which depends primarily on the strength of the mechanical feedback. Interestingly, the three exponents α (for mean squared displacement), λ (for number growth) and ξ (for size growth) are related as $\alpha \approx \lambda \approx 2\xi$, providing evidence that cell dynamics and tissue growth are interrelated. Therefore, we can estimate the values of the other two exponents if one of them is obtained in experiments. The phase diagram summarizing our findings provides a unified picture of the disparate dynamics found in several theoretical studies [11–13]. Because these arguments are general, we propose that global dynamics of a growing cell collectives must exhibit the features of sub-diffusive to hyper-diffusive motion. Finally, it is likely that the non-equilibrium dynamics, due to the interplay between mechanical feedback and $k_b >> k_a$,

may also be relevant in other situations such as embryogenesis and wound healing.

Experimental Validation: The prediction that there is a strong correlation between growth laws of tissues and dynamics of single cells could be validated by we performing experiments along the lines of Puliafito et.al. [5], where MDCK cells were grown on a two dimensional substrate. In the above experiment, both the growth laws, and cell dynamics could be measured. If the experiment could be generalized to cell lines with varying cell doubling times and sensitivity to contact inhibition of proliferation, the predictions in the present study can be experimentally tested.

Acknowledgements: This work was supported by a grant from the National Science Foundation (PHY 23-10639) and the Welch Foundation (F-0019).

Data Availability: The simulation code for the present study was custom generated in MATLAB can be found on google drive [31].

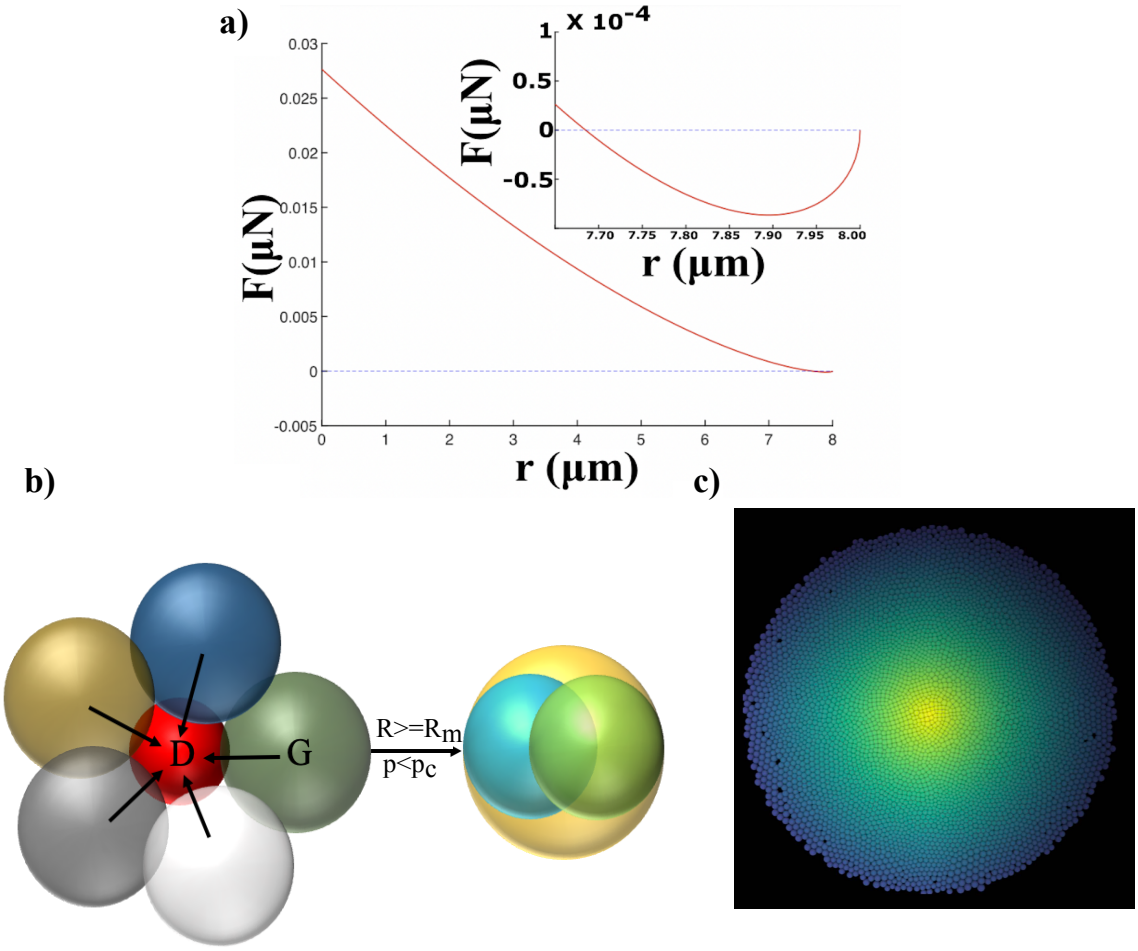

Figure 1: **The 2D model.** (a) Inter-cellular force as a function of distance between two cells with identical radii, $R_i = R_j = 4\mu m$. The repulsive and attractive parts of the force are given by Eqs. (1) and (2), respectively. The inset is the zoomed-in view that highlights the region in which the force is predominantly attractive. (b) Illustration of the role of mechanical feedback. On the left, the "red" cell is dormant (cannot grow and divide) because the pressure exerted by the neighbors exceeds p_c. The "green" cell is in the growth phase (G) ($p < p_c$). The green cell from the left gives birth to two daughter cells (cyan and green) when the radius exceeds the mitotic radius R_m. (c) A snapshot of the 2D growing tissue consisting of approximately 4,750 cells at $t^* = 3.74$, with $p_c = 10^{-3} MPa$ and $\frac{k_b}{k_a} = 20$. The global shape is approximately circular. The colors in plot are for illustration purposes only.

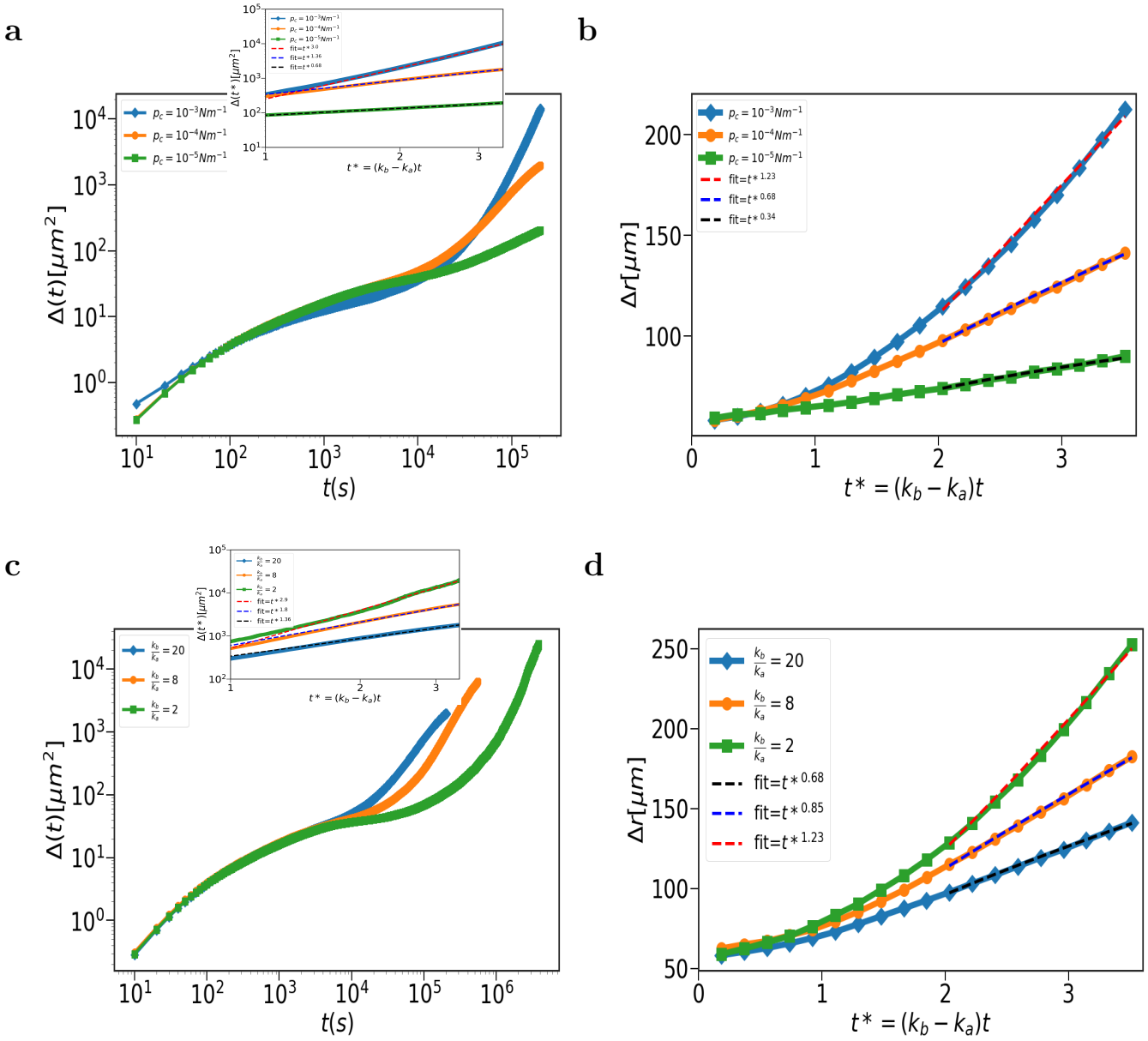

Figure 2: Cell dynamics is regulated by mechanical feedback (p_c) and cell division rate ($\frac{k_b}{k_a}$): (**a**) Mean squared displacement, $\Delta(t)$, as a function of time at fixed $\frac{k_b}{k_a} = 20$. From top to bottom, the curves are for $p_c = 10^{-3} Nm^{-1}, 10^{-4} Nm^{-1}$ and $10^{-5} Nm^{-1}$. The inset focuses on the long time limit ($t > \frac{1}{k_b - k_a}$). The x-axis is scaled by $k_b - k_a$. The dashed lines are power law fits ($\Delta(t) \sim t^{\alpha}$). The α values are given in the upper left box. (Continued on the next page)

Figure 2: (**b**) Size of the cell collective, $\Delta r(t)$ as a function of time for different p_c values at fixed $\frac{k_b}{k_a} = 20$. The dashed lines are power-law fits ($\Delta r \sim (t^*)^{\xi}$). The ξ values are given in the upper left box. (**c**) $\Delta(t)$, as a function of time. From left to right, curves correspond to $\frac{k_b}{k_a} = 20, 8$ and 2 at fixed $p_c = 10^{-4} Nm^{-1}$. The inset focuses on the long time regime ($t > \frac{1}{k_b - k_a}$). The dashed lines are the power law fits ($\Delta(t) \sim (t^*)^{\alpha}$). The α values are given in the upper left box. (**d**) $\Delta r(t)$ as a function of time for changing $\frac{k_b}{k_a}$. The dashed line is the power law fit ($\Delta r \sim (t^*)^{\xi}$). The ξ values are given in the upper left box.

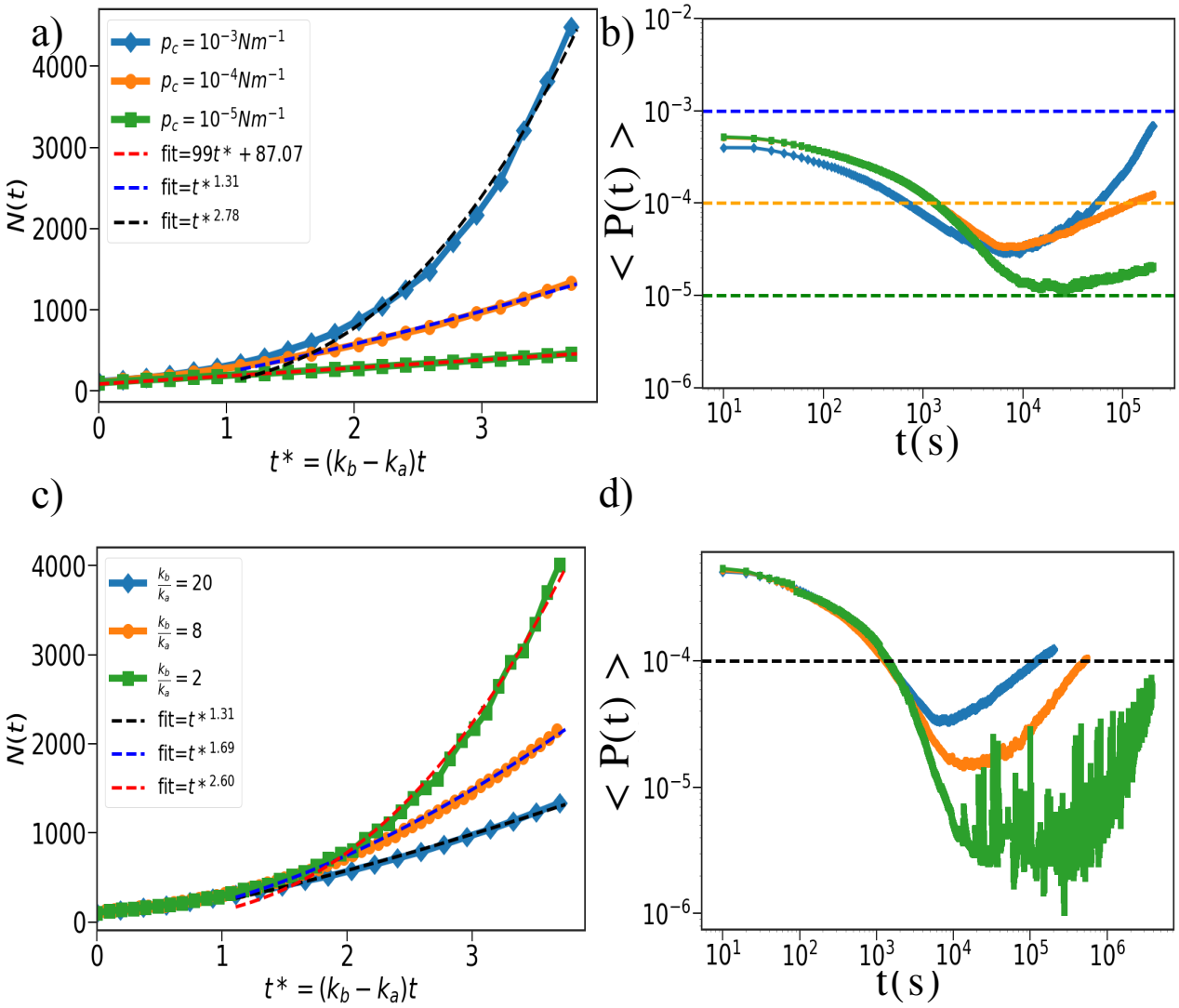

Figure 3: **Growth law governs the cell dynamics:** (**a**) Number of cells, $(N(t))$, as a function of time at three values of p_c, labeled in the figure. The dashed lines with the power the power law fits ($N(t) \sim (t^*)^\lambda$) are shown. (**b**) Average pressure, $\langle P(t) \rangle$, as a function of time. The curves correspond to $p_c = 10^{-3} Nm^{-1} (top), 10^{-4} Nm^{-1}$ (middle), and $10^{-5} Nm^{-1}$ (bottom). The dashed lines mark the p_c values; blue - $p_c = 10^{-3} Nm^{-1}$, orange - $p_c = 10^{-4} Nm^{-1}$, and green - $p_c = 10^{-5} Nm^{-1}$. (Continued on the next page).

Figure 3: (**c**) $N(t)$, as a function of time. From bottom to top, curves correspond to $\frac{k_b}{k_a} = 20$ (blue), 8 (orange) and 2 (green). The dashed lines are the power law fits. The λ values are mentioned in the upper left box. (**d**) Average pressure, $\langle P(t) \rangle$, as a function of time for the three $\frac{k_b}{k_a}$ values. From bottom to top, curves correspond to $\frac{k_b}{k_a} = 20$ (blue), 8 (orange) and 2 (green). The dashed line corresponds to a pressure equal to $10^{-4} N m^{-1}$.

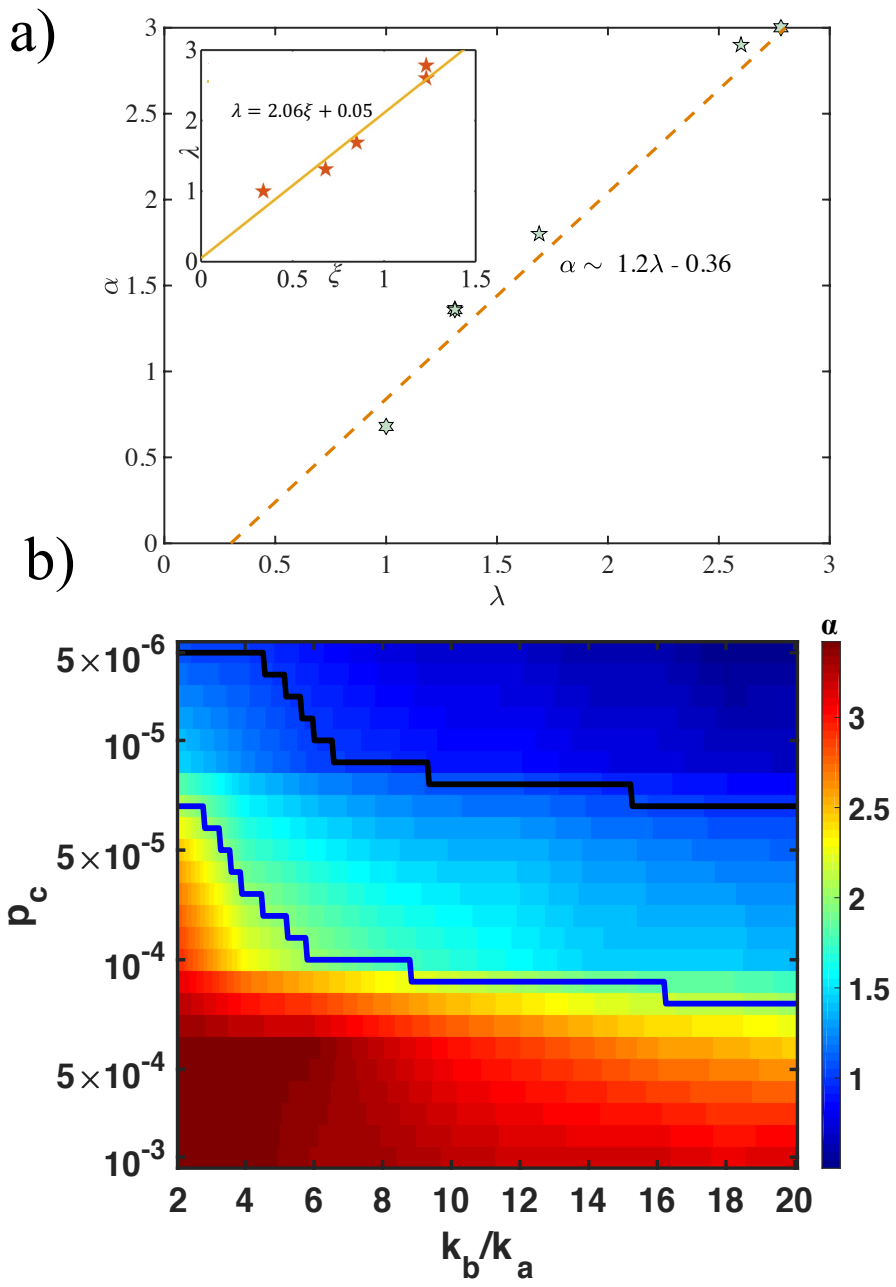

Figure 4: **Dynamical phase diagram :** (a) The MSD exponent α as a function of the growth law exponent λ. The slope of the dashed line is approximately unity. In the inset we plot the relationship between λ and ξ. The fit of the line is $\lambda \approx 2\xi$. (b) Dynamical regimes as a phase diagram in the plane of p_c and $\frac{k_b}{k_a}$. The color bar on the right shows the value of α. Sub-diffusion ($\alpha \leq 1$), superdiffusion ($1 < \alpha \leq 2$), and hyper-diffusion ($\alpha > 2$) in the long-time cell dynamics ($(k_b - k_a)t > 1$). The black (blue) lines correspond to $\alpha = 1$ ($\alpha = 2$).

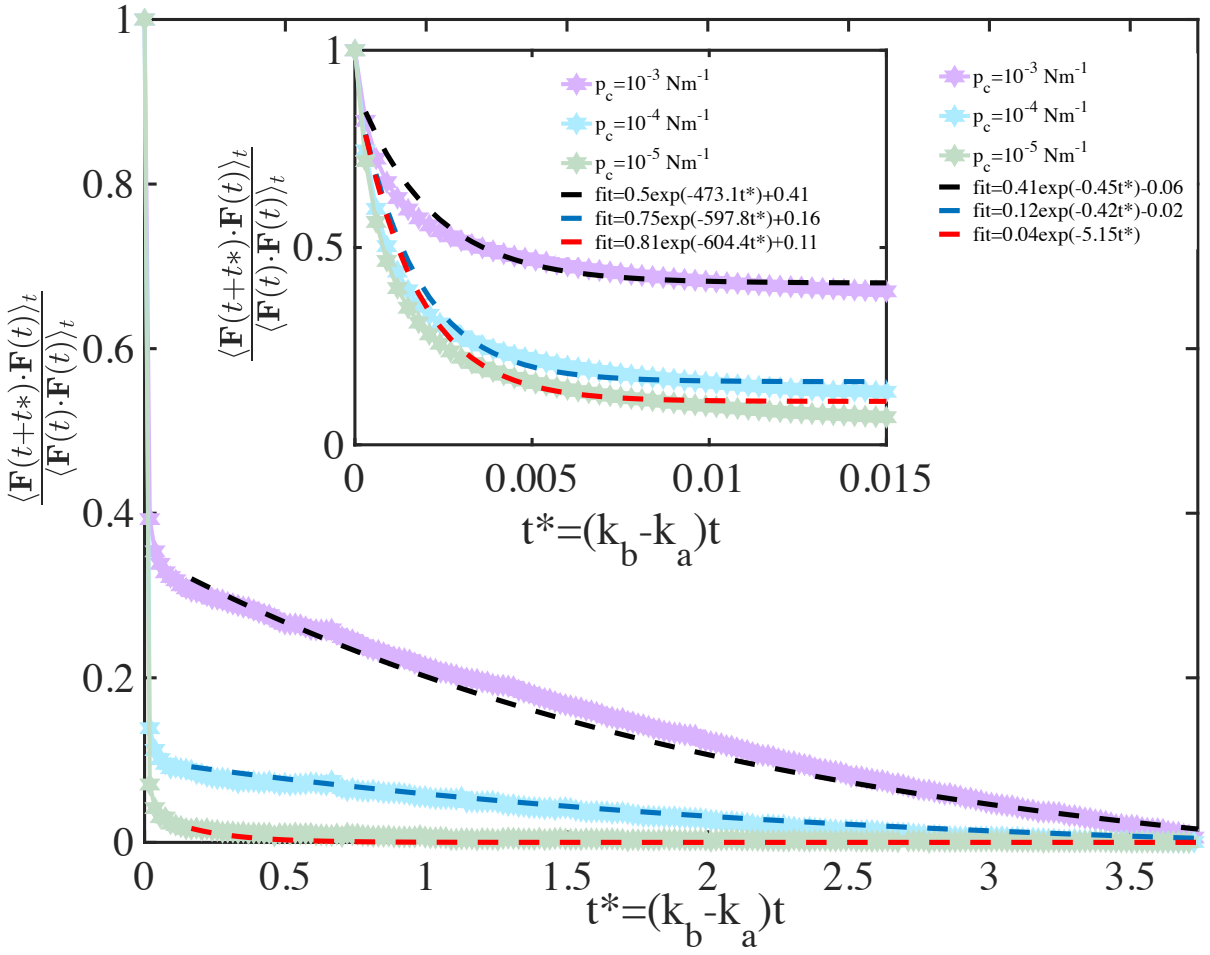

Figure 5: **Correlation in force:** Force autocorrelation function (FAF) as a function of time. From top to bottom, FAF corresponds to $p_c = 10^{-3}, 10^{-4}$ and 10^{-5}. The dashed lines are the fits. Inset is the zoomed of the initial times. The figure shows the emergence of FAF with two-time scales: long ($\sim \frac{1}{k_b - k_a}$) and short (elastic time scale $= \frac{\gamma}{ER}$).

[1] Barres B, Hart I, Coles H, Burne J, Voyvodic J, Richardson W, et al. Cell death and control of cell survival in the oligodendrocyte lineage. Cell. 1992;70(1):31–46.

[2] Lecuit T, Le Goff L. Orchestrating size and shape during morphogenesis. Nature. 2007;450(7167):189.

[3] Weinberg RA. The Biology of Cancer, 2nd Edition. Garland Science; 2013.

[4] Kumar S, Weaver VM. Mechanics, malignancy, and metastasis: the force journey of a tumor cell. Cancer and Metastasis Reviews. 2009;28(1-2):113–127.

[5] Puliafito A, Hufnagel L, Neveu P, Streichan S, Sigal A, Fygenson DK, et al. Collective and single cell behavior in epithelial contact inhibition. Proceedings of the National Academy of Sciences. 2012;109(3):739–744.

[6] Valencia AMJ, Wu PH, Yogurtcu ON, Rao P, DiGiacomo J, Godet I, et al. Collective cancer cell invasion induced by coordinated contractile stresses. Oncotarget. 2015;6(41):43438.

[7] Han YL, Pegoraro AF, Li H, Li K, Yuan Y, Xu G, et al. Cell swelling, softening and invasion in a three-dimensional breast cancer model. Nature physics. 2020;16(1):101–108.

[8] Kim JH, Pegoraro AF, Das A, Koehler SA, Ujwary SA, Lan B, et al. Unjamming and collective migration in MCF10A breast cancer cell lines. Biochemical and biophysical research communications. 2020;521(3):706–715.

[9] Sinha S, Thirumalai D. Self-generated persistent random forces drive phase separation in growing tumors. The Journal of Chemical Physics. 2020;153(20).

[10] Shraiman BI. Mechanical feedback as a possible regulator of tissue growth. Proceedings of the National Academy of Sciences. 2005;102(9):3318–3323.

[11] Czajkowski M, Sussman DM, Marchetti MC, Manning ML. Glassy dynamics in models of confluent tissue with mitosis and apoptosis. Soft matter. 2019;15(44):9133–9149.

[12] Malmi-Kakkada AN, Li X, Samanta HS, Sinha S, Thirumalai D. Cell Growth Rate Dictates the Onset of Glass to Fluidlike Transition and Long Time Superdiffusion in an Evolving Cell Colony. Physical Review X. 2018;8(2):021025.

[13] Matoz-Fernandez D, Martens K, Sknepnek R, Barrat J, Henkes S. Cell division and death inhibit glassy behaviour of confluent tissues. Soft matter. 2017;13(17):3205–3212.

[14] Drasdo D, Höhme S. A single-cell-based model of tumor growth in vitro: monolayers and spheroids. Physical biology. 2005;2(3):133.

[15] Schaller G, Meyer-Hermann M. Multicellular tumor spheroid in an off-lattice Voronoi-Delaunay cell model. Physical Review E. 2005;71(5):051910.

[16] Malmi-Kakkada AN, Sinha S, Li X, Thirumalai D. Adhesion strength between cells regulate nonmonotonic growth by a biomechanical feedback mechanism. Biophysical Journal. 2022;121(19):3719–3729.

[17] Sinha S, Malmi-Kakkada AN, Li X, Samanta HS, Thirumalai D. Spatially heterogeneous dynamics of cells in a growing tumor spheroid: Comparison between theory and experiments. Soft matter. 2020;16(22):5294–5304.

[18] Gniewek P, Schreck CF, Hallatschek O. Biomechanical feedback strengthens jammed cellular packings. Physical review letters. 2019;122(20):208102.

[19] Sinha S, Li X, Das R, Thirumalai D. Mechanical feedback controls the emergence of dynamical memory in growing tissue monolayers. The Journal of Chemical Physics. 2022;156(24).

[20] Nerger BA, Sinha S, Lee NN, Cheriyan M, Bertsch P, Johnson CP, et al. 3D Hydrogel Encapsulation Regulates Nephrogenesis in Kidney Organoids. Advanced Materials.

2024;36(14):2308325.

[21] Yang X, Manning ML, Marchetti MC. Aggregation and segregation of confined active particles. Soft matter. 2014;10(34):6477–6484.

[22] McClatchey AI, Yap AS. Contact inhibition (of proliferation) redux. Current opinion in cell biology. 2012;24(5):685–694.

[23] Eagle H, Levine EM. Growth regulatory effects of cellular interaction. Nature. 1967;213(5081):1102–1106.

[24] Motti ML, Califano D, Baldassarre G, Celetti A, Merolla F, Forzati F, et al. Reduced E-cadherin expression contributes to the loss of p27 kip1-mediated mechanism of contact inhibition in thyroid anaplastic carcinomas. Carcinogenesis. 2005;26(6):1021–1034.

[25] Ranft J, Basan M, Elgeti J, Joanny JF, Prost J, Jülicher F. Fluidization of tissues by cell division and apoptosis. Proceedings of the National Academy of Sciences. 2010;.

[26] Freyer JP, Sutherland RM. Regulation of growth saturation and development of necrosis in EMT6/Ro multicellular spheroids by the glucose and oxygen supply. Cancer research. 1986;46(7):3504–3512.

[27] Casciari JJ, Sotirchos SV, Sutherland RM. Variations in tumor cell growth rates and metabolism with oxygen concentration, glucose concentration, and extracellular pH. Journal of cellular physiology. 1992;151(2):386–394.

[28] Landry J, Freyer JP, Sutherland RM. Shedding of mitotic cells from the surface of multicell spheroids during growth. Journal of cellular physiology. 1981;106(1):23–32.

[29] Galle J, Loeffler M, Drasdo D. Modeling the effect of deregulated proliferation and apoptosis on the growth dynamics of epithelial cell populations in vitro. Biophysical journal. 2005;88(1):62–75.

[30] Godard BG, Heisenberg CP. Cell division and tissue mechanics. Current opinion in cell biology. 2019;60:114–120.

[31] Google Drive Link;. https://drive.google.com/file/d/1UlmwF8sQVJsKF9nCz73NMzIrq9pXb3Rm/view?usp=drive_link.

The simulation code for the present study was custom generated in MATLAB and can be found at -

https://drive.google.com/file/d/1UlmwF8sQVJsKF9nCz73NMzIrq9pXb3Rm/view?usp=drive_link